



Case-inspired exploration of renin mutations in autosomal dominant tubulointerstitial kidney disease: not all paths lead to the endoplasmic reticulum

Joanna Niedbalska-Tarnowska¹ · Anna Jakubowska² · Michał Majkowski³ · Michalina Pęcherz¹ · Anna Medyńska² · Robert Mroczek¹ · Katarzyna Kiliś-Pstrusińska² · Małgorzata Cebrat¹ · Agnieszka Łaszkiwicz¹

Received: 9 October 2023 / Revised: 12 February 2024 / Accepted: 6 March 2024 / Published online: 23 March 2024
© The Author(s), under exclusive licence to International Pediatric Nephrology Association 2024

Abstract

Background Autosomal dominant tubulointerstitial kidney disease (ADTKD) results from mutations in various genes, including *REN*, *UMOD*, *MUC1*, and *HNF1B*. ADTKD due to *REN* mutations (ADTKD-REN) is often characterized as a proteinopathy that triggers the endoplasmic reticulum stress (ERS) cascade, potentially sharing similarities with ADTKD-UMOD and ADTKD-MUC1 at the cellular level. This study, inspired by a patient harboring a W17R mutation, investigates ERS activation by this mutation alongside two other renin variants, W10R and L381P.

Methods We established stable cell lines expressing both wild-type and mutated renin forms (W17R, W10R, and L381P). Using luciferase reporter assays, RT-qPCR, and confocal microscopy, we evaluated ERS activation, determined the cellular localization of the renin variants, and characterized the mitochondrial network in the W17R line.

Results The L381P line exhibited ERS activation, including transcriptional upregulation of *MANF* and *CRELD2*. No ERS activation was observed in the W17R line, while the W10R line exhibited intermediate characteristics. Notably, the W17R variant was misrouted to the mitochondria resulting in changes of the mitochondrial network organisation.

Conclusions ERS activation is not a universal response to different renin mutations in ADTKD-REN. The pathogenesis of the W17R mutation may involve mitochondrial dysfunction rather than the ER pathway, albeit further research is needed to substantiate this hypothesis fully. Testing *CRELD2* and *MANF* as targeted therapy markers for a specific subgroup of ADTKD-REN patients is recommended. Additionally, fludrocortisone treatment has shown efficacy in stabilizing the renal function of our patient over a four-year period without significant side effects.

Keywords Autosomal dominant tubulointerstitial kidney disease · Renin · ADTKD-REN · ADTKD-UMOD · Mitochondrially inherited tubulointerstitial kidney disease (MITKD) · *CRELD2* · *MANF*

Introduction

Autosomal dominant tubulointerstitial kidney disease (ADTKD) represents a spectrum of rare nephrological disorders, characterized by interstitial fibrosis, tubular damage, and often bland urinalysis, leading progressively to kidney failure. The complexity of ADTKD arises from its varied genetic origins, with mutations in such genes as *UMOD*, *MUC1*, *REN*, *SEC61A1*, and *HNF1B*. This genetic diversity, coupled with non-specific clinical presentations, poses a significant diagnostic challenge, requiring comprehensive genetic investigation for accurate diagnosis [1]. In this study, we detail the case of a young patient displaying symptoms of kidney disease, anemia, hyperkalemia, and hypotension,

✉ Agnieszka Łaszkiwicz
agnieszka.laszkiwicz@hirsfeld.pl

¹ Hirsfeld Institute of Immunology and Experimental Therapy, Polish Academy of Sciences, Laboratory of Molecular and Cellular Immunology, Wrocław, Poland

² Department of Pediatric Nephrology, Wrocław Medical University, Wrocław, Poland

³ Faculty of Biotechnology, University of Wrocław, Wrocław, Poland

which raised the suspicion of a mutation in the *REN* gene. Subsequent genetic testing confirmed a W17R substitution in renin, leading to a definitive diagnosis of ADTKD-REN.

Renin, a key player in the renin–angiotensin–aldosterone cascade, is crucial for regulating nephrogenesis, erythropoiesis, blood pressure, and fluid balance. Primarily synthesized in the granular cells of the juxtaglomerular apparatus, renin originates as preprorenin. It undergoes processing in the endoplasmic reticulum (ER) where its signal peptide is cleaved, forming prorenin. Prorenin then navigates through the secretory pathway and can be either secreted directly or further processed into active renin. Interestingly, besides its conventional role in the kidneys, renin also influences local renin–angiotensin systems in various organs. Investigations into these systems have uncovered alternative renin transcripts lacking exon 1, which encodes the signal peptide. They bypass the ER and are translated by free ribosomes, leading to a form known as intracellular renin (renin b). Notably, renin b can be directed to the mitochondria, although its specific function in this location is still being investigated [2–7].

Certain mutations in renin can halt its synthesis completely. While heterozygous carriers of these mutations are usually not significantly affected, homozygous individuals develop severe renal tubular dysgenesis (RTD [MIM# 267430]), often resulting in perinatal death [8]. Therefore, dominant renin mutations linked to ADTKD-REN are thought to induce a gain-of-function effect, predominantly due to the accumulation of malfunctioning proteins within cells, a consequence of disrupted transport processes.

The nature of these intracellular trafficking abnormalities varies with the location of the mutation, as shown in a recent international cohort study. Mutations within the *REN* signal peptide, such as the W17R variant, typically impede translocation across the ER membrane, leading to the accumulation of non-glycosylated preprorenin in the cytoplasm. Conversely, mutations in the mature renin and prosegment sections result in protein accumulation within the endoplasmic reticulum and the ER–Golgi intermediate compartment (ERGIC), respectively [9].

The mechanisms by which disruptions in renin protein processing and transport lead to cellular toxicity and chronic kidney disease are not fully understood. While research on ADTKD-UMOD and ADTKD-MUC1 has emphasized the role of endoplasmic reticulum stress (ERS) and the unfolded protein response (UPR) [1], the involvement of these pathways in ADTKD-REN, particularly with signal sequence mutations like W17R, remains less explored [10]. Investigating the ERS activation by W17R and similar mutations is crucial, as it represents one of the targets in ongoing molecular therapy research [11, 12]. Understanding these common

molecular pathways is key to expanding treatment options for a broader patient group.

Our study aims to explore whether ERS can be a universal response to various renin mutations in ADTKD-REN, including W17R. To this end, we utilized HEK293T-derived cell lines expressing both wild-type renin and its mutated forms. Our analysis includes the patient's specific mutation, W17R, as well as the W10R variant, with the L381P mutation serving as a control due to its established association with ER stress [13].

Moreover, our investigation extends to assessing the potential mitochondrial localization of the W17R renin variant. This endeavor was inspired by the observation of intracellular renin's mitochondrial localization and the intriguing correlation between mitochondria and ADTKD. Specifically, an atypical form of TKD known as mitochondrially inherited tubulointerstitial kidney disease (MITKD), linked to mitochondrial DNA (mtDNA) mutations, leads to the ADTKD phenotype [14]. We hypothesized that if W17R targets the mitochondria, it might suggest a potential molecular similarity with MITKD and unveil a novel direction in the exploration of ADTKD-REN mechanisms.

Additionally, we examine the long-term effects of fludrocortisone treatment in a patient with the W17R renin mutation. This treatment, suggested for managing aldosterone deficiency in ADTKD-REN [15], has limited documentation in prolonged use cases. Our study not only presents these clinical findings but also contributes to a deeper understanding of the pathogenic mechanisms of ADTKD-REN, aiming to pave the way for patients with ADTKD-REN to benefit from emerging mechanism-based therapies.

Materials and Methods

Genetic evaluation

Genomic DNA was extracted from buccal swabs using GenemATRIX Swab-Extract DNA Purification Kit (Euryx). Exon 1 of the *REN* gene was amplified by PCR and subsequently subjected to Sanger sequencing. Additionally, amplicons were cloned into the pGEM®T easy vector (Promega) following the manufacturer's protocol. Several clones from each tested individual were sequenced to validate the presence of both wild-type and mutant forms of the *REN* gene in affected individuals. All patients provided informed consent for genetic testing. To illustrate the position of the identified *REN* mutation in relation to the signal peptide regions (Online Resources 4), SignalP 6.0 was used to predict the N-terminal region, the hydrophobic central region, and the C-terminal region [16].

Cell culture

HEK-293 T (CRL-3216) cell line was purchased from the American Type Culture Collection (ATCC, Manassas, VA, USA), LentiX-293 T was from the Hirszfeld Institute of Immunology and Experimental Therapy, Polish Academy of Sciences (HIIET, PAS, Wrocław, Poland), while HMC1 was a generous gift from Dr A. Walczak–Drzewiecka, Institute of Medical Biology of Polish Academy of Sciences, Łódź, Poland.

HEK-293 T and HEK LentiX were cultured in DMEM medium (HIIET, PAS, Wrocław, Poland) supplemented with 2 mM glutamine, 4.5 g/L glucose, and 10% FBS (Sigma–Aldrich, St. Louis, MO, USA). HMC-1 mast cells were cultured in IMDM (HIIET, PAS, Wrocław, Poland) supplemented with 10% heat-inactivated FCS, and 4 mM L-glutamine [17]. All cell lines were propagated under standard conditions at 37 °C in a humidified atmosphere containing 5% CO₂.

Construction of expression vectors coding for wild-type hREN and its mutated forms

The *hREN* cDNA was obtained through reverse transcription of RNA extracted from HMC1 cells [18] followed by PCR amplification using Platinum™ SuperFi II Green PCR Master Mix (Invitrogen). The primer sequences were designed to include the restriction sites (HindIII and BamHI) required for cloning into the pcDNA3 vector (Invitrogen). Plasmids were propagated in *Escherichia coli* HST08 cells (Takara), and the correct clones were selected based on sequencing analysis.

Mutant constructs were generated through site-directed mutagenesis using Platinum™ SuperFi polymerase and overlapping mutagenic primers with 3′-overhangs, following the manufacturer's recommendations (Invitrogen).

Both the wild-type and mutated versions of the *hREN* gene were amplified by PCR and then cloned into pRRL-CMV-IRES-PURO – a self-inactivating lentiviral expression vector [19] – via MluI and XhoI restriction sites, using standard cloning techniques. The resulting plasmids were propagated in *Escherichia coli* NEB® Stable strain at a reduced temperature (30 °C), and the sequences of the inserts were confirmed by Sanger sequencing.

The constructed expression vectors were designated as pRRL-RenWT, pRRL-RenW10R, pRRL-RenW17R, and pRRL-RenL381P.

Lentiviral transduction of HEK293T cell line

Lentiviral particles were generated through transient transfection of approximately 3×10^6 HEK293T LentiX cells

with 6 µg of one of the expression vectors (pRRL-RenWT, pRRL-RenW10R, pRRL-RenW17R or pRRL-RenL381P), 3 µg of pMDL-g/p-RRE (a gift from Didier Trono: Addgene plasmid #12,251), 1.5 µg of pRSV-REV (a gift from Didier Trono: Addgene plasmid #12,253) [20] and 1.5 µg of pMk-VSVG [19] using Transporter 5 Transfection Reagent (Polysciences). After 18–24 h the medium was changed. Culture supernatants containing viral particles were collected 48–72 h after transfection, clarified through a 0.45 µm pore size filter (Millipore), and used for the transduction of HEK293T cells. Approximately 5×10^4 cells were exposed to viral particles present in the culture supernatant (3 ml), along with polybrene (8 µg/mL, MilliporeSigma™), via centrifugation ($367 \times g$) for 80 min at room temperature, followed by an overnight incubation period. Subsequently, the medium was replaced, and puromycin selection (2 µg/mL) was implemented on both transduced cells and non-transduced control cells to ensure the cultivation of only stably transfected cells. Cells selected for their consistent expression of the specified protein versions were labeled as WT, W10R, W17R, and L381P cell lines.

RNA isolation and reverse transcription

RNA from the cell lines was isolated using the ExtractME Total RNA Kit (BLIRT) following the manufacturer's instructions, with an additional digestion step using the TURBO DNA-free™ Kit (Thermo Fisher Scientific). After assessing its quality on an agarose gel, 5 µg of RNA was reverse-transcribed following the manufacturer's instructions for Superscript IV (Invitrogen).

RT-qPCR analyses

RT-qPCR analyses were conducted using the PowerUp™ SYBR™ Green Master Mix (Applied Biosystems™) on the QuantStudio™ 3 Real-Time PCR System (Applied Biosystems™). The following steps were performed: an initial hold stage (50 °C for 2 min, 95 °C for 2 min), 40 cycles of amplification (94 °C for 15 s, 60 °C for 1 min), and a melt curve stage (95 °C for 15 s, 60 °C for 1 min, 95 °C for 15 s).

Each reaction utilized one microliter of cDNA or a non-reverse-transcribed negative control. The primer sequences for amplifying the tested and control genes are available in Online Resource 1. Standard curves for each primer set were established using a series of fivefold dilutions of one of the template cDNAs. The expression levels of the analysed genes were normalized to an endogenous control and presented in relation to non-treated HEK 293 T cells, for which gene expression was arbitrarily set as 1. Product specificity was confirmed through melting curve analysis.

Luciferase assay

Reporter constructs were obtained from Addgene: ATF6 ("p5xATF6-GL3") was generously provided by Ron Prywes (Addgene plasmid #11,976) [21], ATF4 ("Mouse ATF4 (CHOP11/cATF), 5'UTR and AUG-luc") was a kind gift from David Ron (Addgene plasmid #21,850) [22], and XBP1 ("pFLAG-XBP1u-FLuc") was generously provided by Jim-tong Horng (Addgene plasmid #31,239) [23].

The WT, W10R, W17R, and L381P cell lines were seeded in 24-well plates at a density of 17×10^4 cells per well. The following day, they were transfected with one of the reporter constructs: ATF6 (300 ng), ATF4 (455 ng), or XBP1 (500 ng) using Transporter 5 Transfection Reagent (Polysciences, Inc, Warrington, PA, USA). Additionally, for ATF6 and ATF4 constructs, a pRLTK plasmid (45 ng) encoding *Renilla* luciferase was co-transfected to serve as an internal control. After 48 h of transfection, the cells were lysed, and their firefly and *Renilla* luciferase activities were assessed using the Dual-Luciferase® Reporter Assay System (Promega) and a Luminometer TD-20/20 (Turner Designs). As a positive control, cells were induced with tunicamycin (2.5 µg/ml, SIGMA) for 20 h prior to the measurement.

SDS-PAGE and western blot

The western blot analysis was conducted on both the culture media and cell lysates of the WT, W17R, W10R, L381P, and NT lines. A detailed protocol, including the antibodies used, is provided in Online Resource 2.

Renin activity measurement

Cells were seeded in 24-well plates (25×10^4 cells/well). On the following day, the medium was substituted with fresh low serum medium (1.7% FBS) devoid of phenol red. After 24 h, the activity of the renin secreted into the medium was assessed using Sigma-Aldrich Renin Assay Kit (MAK157). Before measurement, renin was activated through trypsin treatment: 25 µl of the medium was incubated at 37 °C for 20 min in a 50 µl assay buffer reaction containing 0.4 µg of trypsin. The reactions were stopped by adding 1 µl of 100 mM PMSF. Subsequently, 50 µl of diluted renin substrate was introduced, and the fluorescent signal ($\lambda_{ex} = 540/\lambda_{em} = 590$) was monitored every 5 min for 130 min at 37 °C using Synergy H4 Hybrid Reader.

Immunofluorescence

The immunofluorescence method was used to determine the localization of prorenin in cells and in the analysis of mitochondrial network morphology. Detailed procedures

for preparation of samples, including the specific antibodies used and the conditions under which images were obtained, are described in the Online Resource 2.

Colocalization analysis

The colocalization of renin with the ER marker P4HB, as well as renin with mitochondria (MitoTracker™), was quantified using the JACoP plugin in FIJI [24, 25].

Cells revealing high signal originating from renin were chosen for the colocalization measurement. Before the colocalization measurement both analysed images (showing ER and renin) were filtered using Gaussian Blur filter with sigma parameter (radius) set to 1 pixel. Colocalization was expressed as Mander's Coefficients (which represent fraction of renin overlapping ER) determined for thresholded images. Thresholds were set manually for each image to cover regions showing the most intense fluorescence signals.

The measurement of the colocalization between renin and mitochondria labeled with MitoTracker was also conducted on individual cells. In this case, colocalization was determined using the Pearson's correlation coefficient.

Mitochondrial morphology and network analysis

The initial assessment of mitochondrial morphology involved counting cells exhibiting small, tubular, or round mitochondrial structures. Calculations were performed on five regions from each investigated group, encompassing a minimum of 30 cells in each region.

3D analysis of the mitochondrial network was conducted using the Mitochondria Analyser plugin within the ImageJ software [25–27], according to the pipeline presented in Online Resource 3.

Statistical analysis

The statistical analysis was conducted using the Microsoft Excel program with the addition of the Real Statistics Resource Pack software (Release 6.8), copyright (2013–2020) Charles Zaiontz. The type of statistical test used, the number of experiment replicates, and the p-value have been detailed in the descriptions of figures presenting the results of each specific experiment.

Results

Clinical findings

A ten-year-old boy, born at 36 weeks of gestation with a body mass of 2460 g, was in good condition. Early childhood

urine sediment tests were normal, showing no proteinuria, and abdominal ultrasound revealed no abnormalities. Since the age of one, he had been under hematological care for anemia, responding temporarily to iron supplementation. His psychomotor development was normal. Family history noted his father had gout, and his paternal grandfather had both gout and chronic kidney disease (CKD) stage 5.

At six years old, he was admitted to our department with a mild fever and minor gastrointestinal symptoms. Laboratory tests indicated high inflammatory parameters (C-reactive protein 240.4 mg/l, procalcitonin 6.7 ng/ml), signs of kidney injury (urea 149.8 mg/dl, creatinine 1.4 mg/dl, uric acid 13.9 mg/dL), anemia (hemoglobin level of 8.7 g/dl), electrolyte imbalances (hyponatremia and hyperkalemia), and metabolic acidosis. Low blood pressure (86/50 mmHg) was also observed. Treatment included antibiotics, intravenous fluids, and rasburicase. Although there was initial improvement, kidney injury parameters worsened and blood pressure remained low upon cessation of intravenous hydration.

Further investigation revealed low levels of plasma renin activity and aldosterone. A 24-h urine collection indicated low aldosterone levels, hypouricosuria, and increased sodium loss. Genetic testing confirmed a heterozygous c.49 T>C sequence variant in exon 1 of the *REN* gene, leading to a diagnosis of autosomal dominant tubulointerstitial kidney disease (ADTKD-REN, W17R) (Online Resource 4). Treatment with allopurinol, increased fluid intake, a high-salt diet with potassium limitation, and fludrocortisone (100 µg per day) was initiated, alongside qualification for darbepoetin therapy. This led to gradual normalization of blood test results and general condition. The decision was made to continue treatment to maintain normal blood pressure.

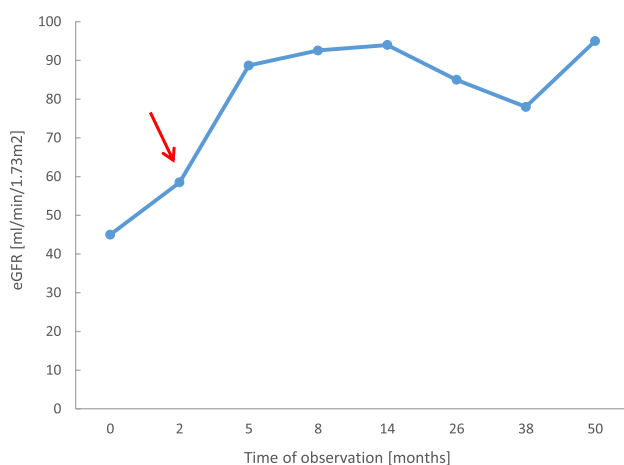


Fig. 1 Estimated glomerular filtration rate (eGFR) in a patient with W17R mutation before and after fludrocortisone treatment. GFR was estimated according to the Schwartz formula. The red arrow indicates the treatment initiation

Currently, four years post-initiation of fludrocortisone treatment, the patient demonstrates stable kidney function (Fig. 1), with no serious side effects noted during therapy. He undergoes regular ophthalmological exams and densitometry, maintains a correct carbohydrate balance, and his growth is appropriate for his age. In 2020, this case was included for statistical analysis in an international cohort study [9], but the specific data presented here were not included in that article (Online Resource 5).

Molecular investigations

Characterization of REN variants stably expressed in HEK293T cells

We established polyclonal cell lines expressing wild-type renin and its mutated forms: W17R, W10R, and L381P. The expression of renin was confirmed and quantitatively evaluated using RT-qPCR. Although the REN mRNA levels varied over time in culture, the difference between cell lines did not exceed 2.5 times (not shown). Western blot analysis verified the presence of renin protein within the cells, showing similar levels of total renin expression across lines (Fig. 2A, Fig. 2B), and revealed reduced secretion into the media for the W10R mutation, while the W17R and L381P forms exhibited no detectable secretion (Fig. 2A). This pattern was corroborated by measuring renin activity in the media (Fig. 2C). Immunofluorescence analysis showed the strongest colocalization with the ER marker (P4HB) for L381P renin, confirming the previously reported retention of this form in the ER [13]. There was no colocalization of W17R with the ER, while the signal overlap level for W10R was similar to that of WT (Fig. 3). The lack of colocalization of the W17R variant with the ER in our cell line aligns with previous reports indicating that this form is not transported to the ER [9]. This observation also corresponds well with the results of the western blot analysis, where only the preprorenin form was observed in W17R cells (Fig. 2A, 2B, Online Resource 6).

Evaluation of the activation of the ER stress markers

To assess the potential induction of ER stress by the W17R and W10R variants of renin, we examined the major markers of unfolded protein response (UPR) in cell lines where the wild-type or mutated forms of this protein were stably expressed. For comparison, we included a cell line expressing the L381P version of renin, as its ability to activate the UPR has been previously demonstrated in a cellular model [13]. The utilization of Xbp1, ATF4, and ATF6 luciferase reporter constructs [21–23] enabled us to assess the activity of the major upstream regulators of the three unfolded

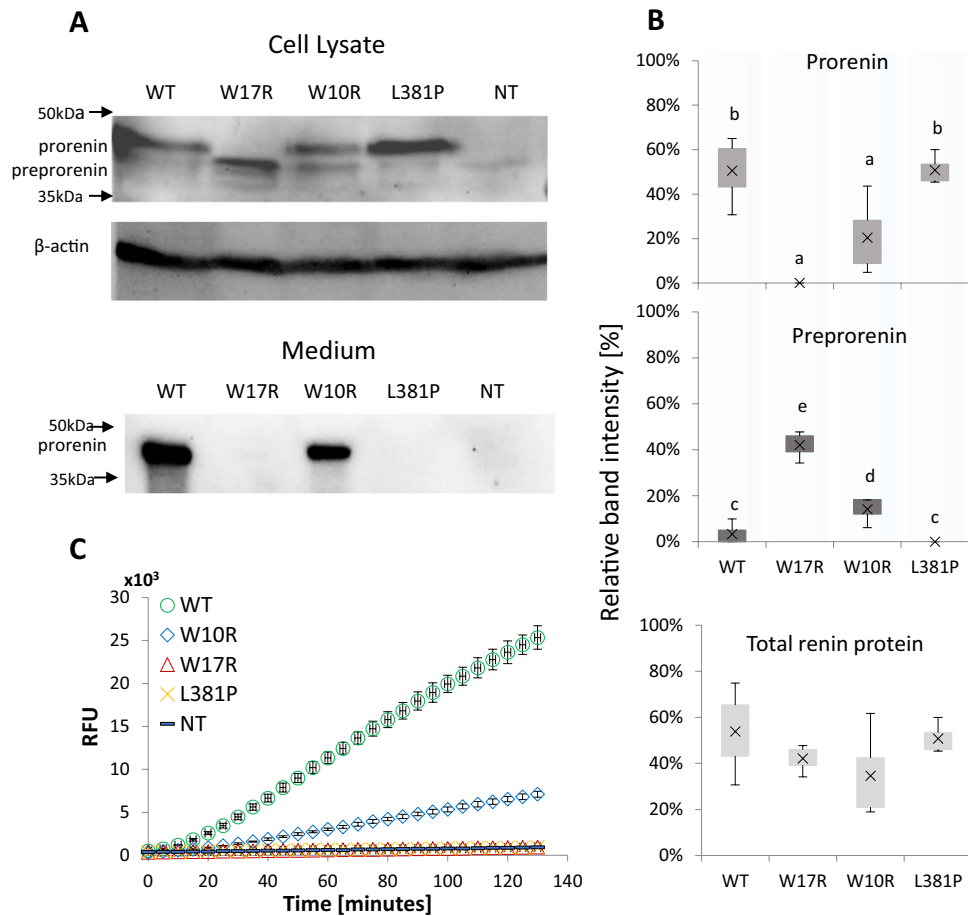


Fig. 2 The renin variants expression in WT, W17R, W10R, and L381P cell lines. **A** Western blot analysis of renin in cell lysates and cell culture media detected using rabbit anti-prorenin serum (265–294, Yanaihara Institute); β -actin is presented as a loading control. 'NT' stands for non-transduced HEK293T cells. **B** Relative expression levels of prorenin and preprorenin in cell lysates of WT, W17R, W10R, and L381P lines. Band intensities for prorenin or preprorenin were normalized against the β -actin signal. Results are presented as mean values ($n=3$) \pm standard deviation. Due to the lack of normal distribution, the statistical significance of differences in prorenin and preprorenin levels was determined using the Kruskal–Wallis test

followed by Conover's post hoc test. The letters (a, b, c, d, e) depict groups with statistically different values ($p < 0.05$). Total renin protein expression was quantified by summing the intensities of prorenin and preprorenin bands relative to the β -actin signal, with results shown as mean values ($n=3$) \pm standard deviation. The statistical significance of the total renin expression differences was evaluated using ANOVA. **C** Activity of the renin secreted into the medium (after trypsin treatment). The fluorescent signal, resulting from the cleavage of the renin substrate, was monitored for 130 min, expressed in Relative Fluorescence Units (RFU), and presented as mean values ($n=3$) \pm standard deviation

protein response (UPR) pathways: IRE1, PERK, and ATF6 [28]. In our experiments, the expression of the renin W17R variant did not result in the activation of any of these pathways. In contrast, the control L381P line exhibited signs of activation across all three pathways, whereas the W10R line specifically activated the PERK pathway (as indicated by reporter ATF4) (Fig. 4A). Using RT-qPCR, we observed increased expression of the *HSPA5* gene, which encodes BiP (Immunoglobulin heavy chain-binding protein) – a central regulator of UPR stress sensors, as well as two downstream UPR markers: *CRELD* and *MANF*, but only in the L381P line (Fig. 4B).

Mitochondrial localization of W17R renin and mitochondrial network analysis in the W17R cell line

To test whether W17R renin can be directed to mitochondria, we performed confocal microscopy analysis, which confirmed the partial colocalization of the signals from the anti-renin antibody and the MitoTracker™ (Fig. 5).

Confocal microscope images also revealed variations in mitochondrial morphology among the analysed cell lines: WT, W17R, and the non-transduced HEK293T (NT) control. Three distinct morphological categories were tentatively identified as "rounded," "tubular," and "small" (Fig. 6A). In the NT control line, elongated mitochondria

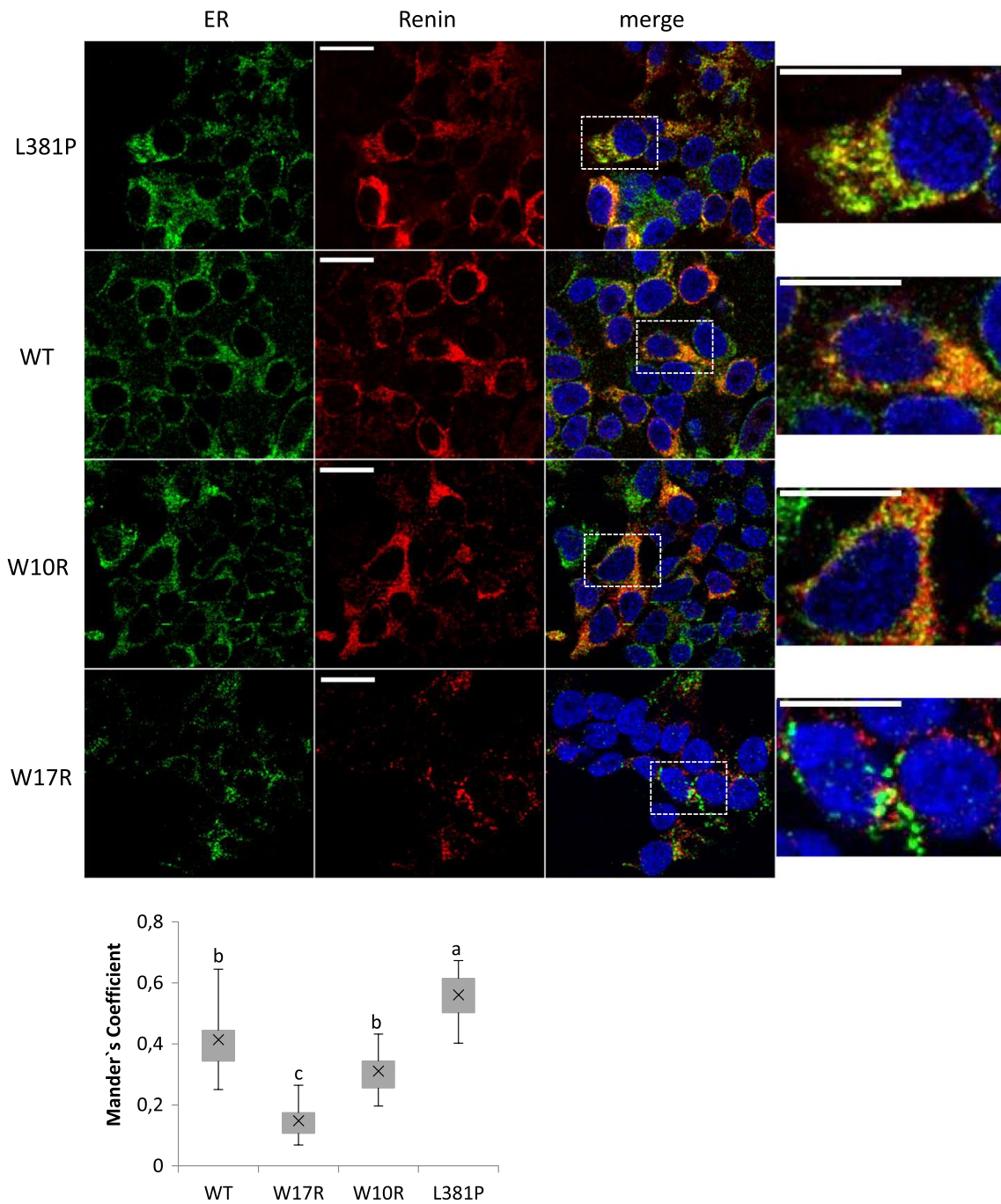


Fig. 3 Localization of renin variants relative to the endoplasmic reticulum (ER). Immunofluorescence analysis conducted on WT, W17R, W10R, and L381P cell lines showing the localization of ER marker (polyclonal rabbit anti-P4HB antibody, green), renin (REN, mouse anti-renin antibody, red), and nuclei (DAPI, blue). Scale bar = 15 μ m.

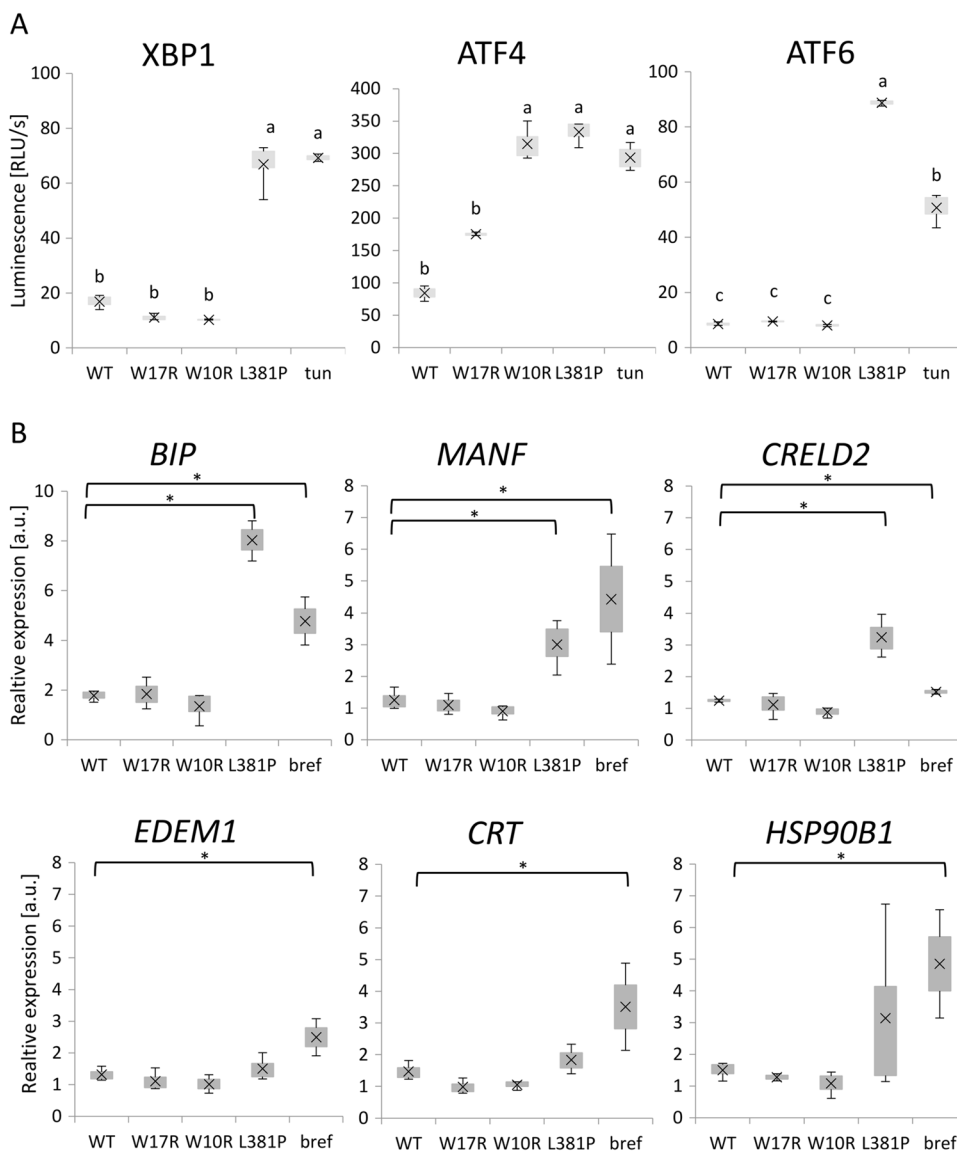
The graph below depicts Mander's coefficients between ER and renin signals. The letters (a, b, c) depict groups with statistically different values ($p < 0.05$), as determined by ANOVA with Games-Howell post hoc test; \pm SD; SD, standard deviation

with a complex tubular network predominated. These cells constituted a notably smaller proportion in the remaining groups, not only in W17R but also in the WT cell line. Cells displaying rounded mitochondria represented a significantly larger population within the WT cells, while the most

prominent characteristic of the W17R line was the highest, statistically significant percentage of cells with small mitochondria (Fig. 6A).

To provide a more precise characterization of mitochondrial morphology within distinct categories, randomly

Fig. 4 Evaluation of ER stress markers activation in WT, W17R, W10R, and L381P cell lines. **A** Detection of XBP1 splicing, ATF6, and ATF4 activation using luciferase-based reporter constructs. Luciferase activity is presented as mean values ($n=3$) \pm standard deviation of relative light units per second (RLU/s). HEK293T cells treated with tunicamycin (2.5 μ g/ml) served as the positive control (tun). The letters (a, b, c) depict groups with statistically different values ($p < 0.05$), as determined by ANOVA with Games-Howell post hoc test. **B** RT-qPCR analysis of ER stress markers: mRNA levels of *BIP* (Binding immunoglobulin protein), *MANF* (Mesencephalic astrocyte-derived neurotrophic factor), *CRELD2* (Cysteine-rich with epidermal growth factor (EGF)-like domains 2), *EDEM1* (ER degradation-enhancing alpha-mannosidase-like protein 1), *CRT* (Calreticulin), and *HSP90B1* (heat shock protein 90 beta family member 1), normalized to *HPRT1* (Hypoxanthine Phosphoribosyltransferase 1). HEK293T cells treated with brefeldin (2.5 μ g/ml) served as the positive control (bref). A.U. = arbitrary unit; \pm SD ($n=3$); the asterisk depicts statistically different groups ($p < 0.05$) from the WT cell line (Student's t-test)



selected cells from each experimental group underwent 3D analysis using the Mitochondria Analyser plug-in within the ImageJ software (Fig. 6B). Additionally, a pool of cells in the anaphase of the cell cycle selected from the NT group was included in the analysis. Taguchi et al. [29] observed that the mitochondrial network in metaphase and anaphase human cells exhibits a higher degree of fragmentation compared to interphase cells. Therefore, the dividing cells were included as an additional control to assist in our analysis of mitochondrial network fragmentation features. As expected, these cells showed a decrease in both mitochondrial mean volume and mean surface area. However, we did not observe other hallmarks of fragmented mitochondrial networks, such as an increase in the number of mitochondria per cell or changes in their sphericity [26]. The W17R cell line did not significantly differ from NT cells in any of these parameters (Fig. 6B).

The structure of the mitochondrial network was described using parameters such as the number of mitochondrial branches, branch length, and the average branch diameter (Fig. 7A). The total branch length and the total branch length per mitochondrion were the lowest and significantly different ($p < 0.01$) in dividing cells, as expected for cells with fragmented mitochondrial networks. However, this decrease in branch length was not accompanied by a reduction in the number of branches. The only parameter in which the W17R line differed statistically from all control cell lines was the average branch diameter, which was significantly lower even when compared to dividing cells (Fig. 7A).

Although the 2D microscope images showed some features of mitochondrial network disruption in renin W17R expressing cells (decreased number of tubular mitochondria and increased number of small mitochondria) (Fig. 6A), the

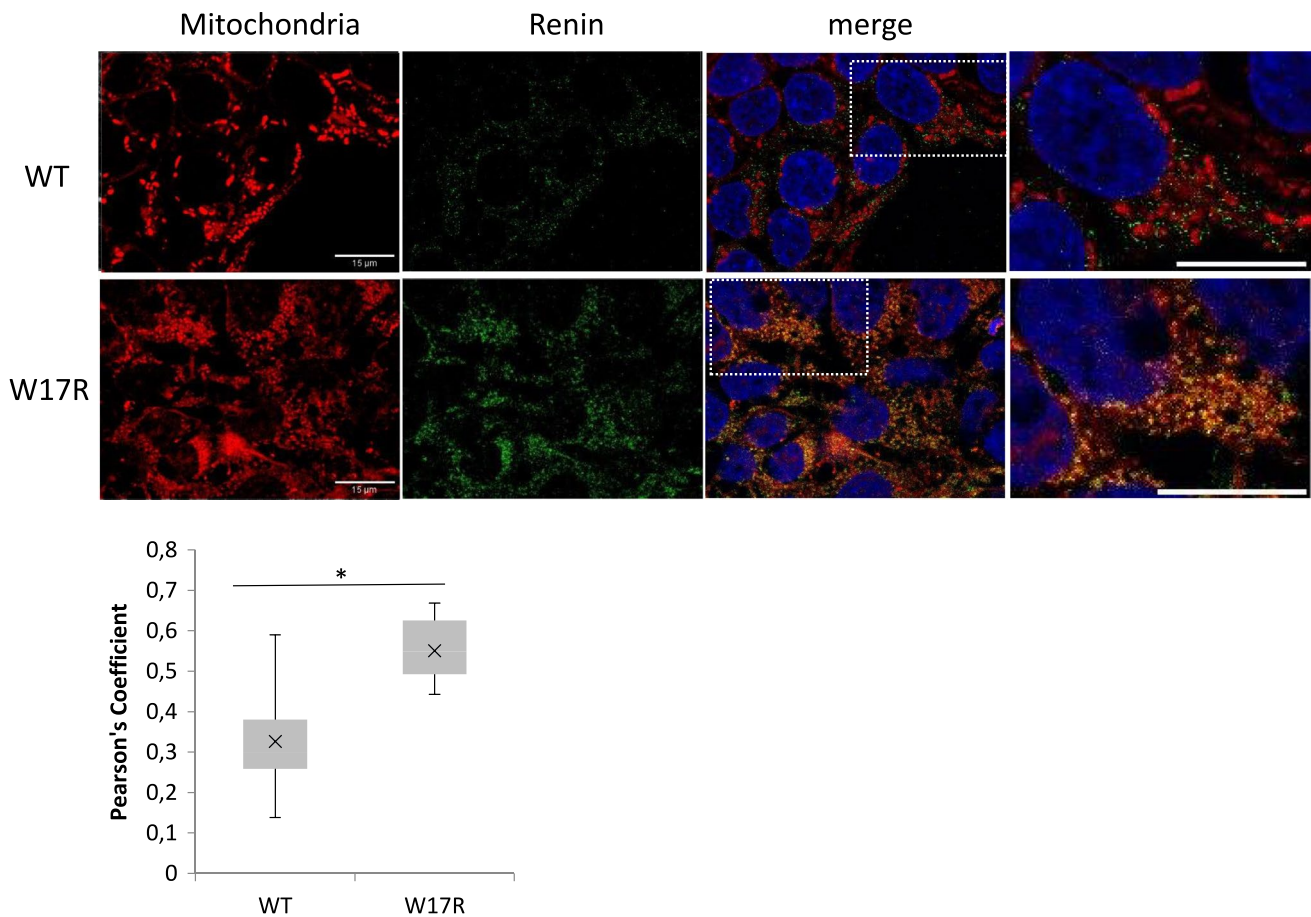


Fig. 5 Intracellular localization of W17R renin. Immunofluorescence analysis revealing the colocalization (merged yellow signals) of W17R renin (green, rabbit anti-prorenin 265–294 serum) with MitoTracker™ (red). Scale bar=15 μm. The graph below depicts

Pearson's correlation coefficient between MitoTracker™ and renin signals ($n=3 \pm$ standard deviation). The asterisk depicts statistically different ($p < 0.05$) groups (Student's t-test)

3D analysis of network morphology did not provide conclusive evidence of whether it can be described as fragmented. Therefore, we conducted RT-qPCR to assess the expression levels of genes encoding proteins involved in fusion, such as optic atrophy 1 (OPA1) and mitofusin 1/2 (MFN1/2), as well as proteins participating in fission, such as dynamin-related protein 1 (DNM1L) and mitochondrial fission protein 1 (FIS1) [30, 31]. Across all cell lines, including W10R and L381P, which were included for comparison purposes, we did not observe any statistically significant differences in the mRNA levels of genes associated with the dynamic processes of the mitochondrial network (Fig. 7B).

Discussion

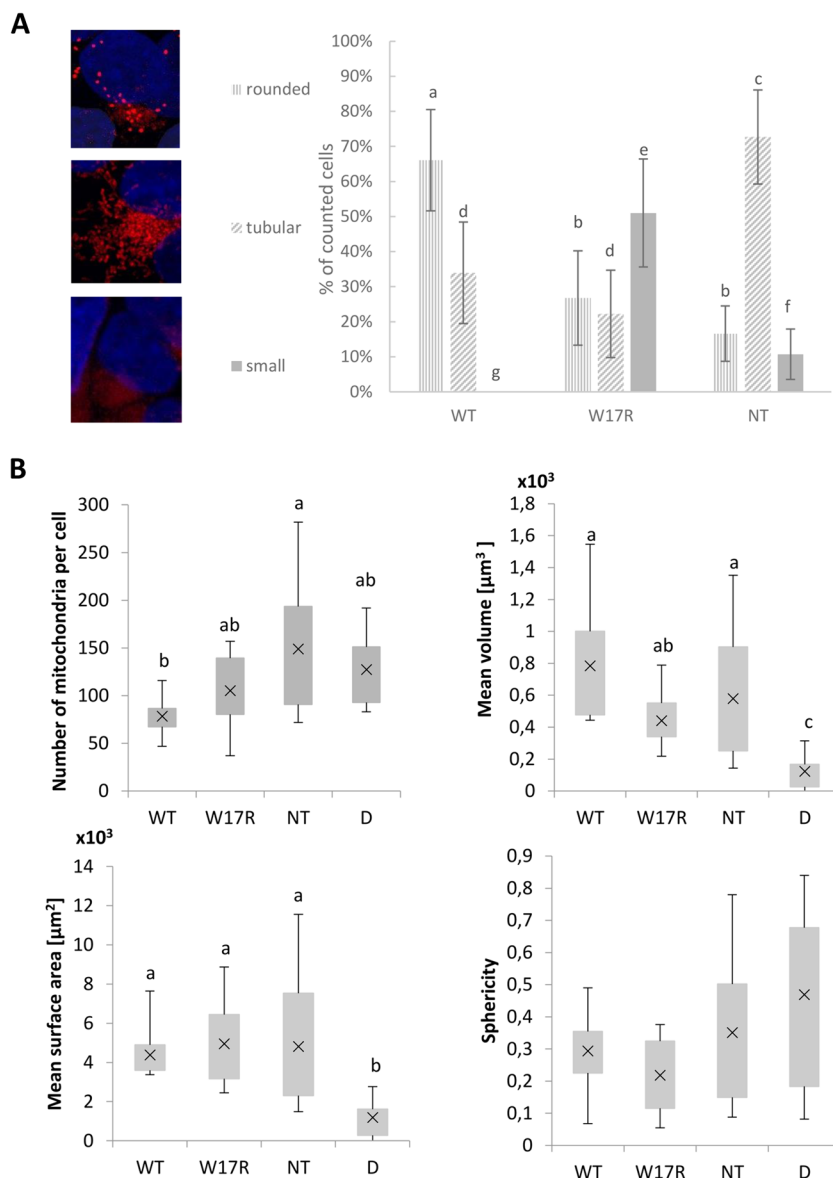
Molecular evidence increasingly highlights how disruptions in protein trafficking through the secretory pathway, and the subsequent induction of ERS, contribute to the pathogenesis of rare kidney diseases, including ADTKD-UMOD and

ADTKD-MUC1. This critical insight has driven the development of mechanism-based therapies, potentially beneficial for a spectrum of diseases affecting not only the kidneys but also other organs [12, 32].

Despite being classified within this disease group, ADTKD-REN exhibits significant heterogeneity in its pathophysiology. For instance, mutations in the mature part of renin, such as the L381P variant, often lead to protein retention in the ER and subsequent activation of ERS, similar to what is observed in ADTKD-UMOD [9, 13]. Our study, utilizing a stable L381P renin expression model, confirmed the potential of this variant to induce the IRE1 and ATF6 branches of the UPR pathway. Interestingly, we also observed activation of the PERK branch, a novel finding that suggests the need for further investigation into model-dependent variations.

A significant discovery in our research was the transcriptional upregulation of *MANF* (encoding mesencephalic astrocyte-derived neurotrophic factor) and *CRELD2* (encoding cysteine-rich with EGF-like domains 2) in the L381P

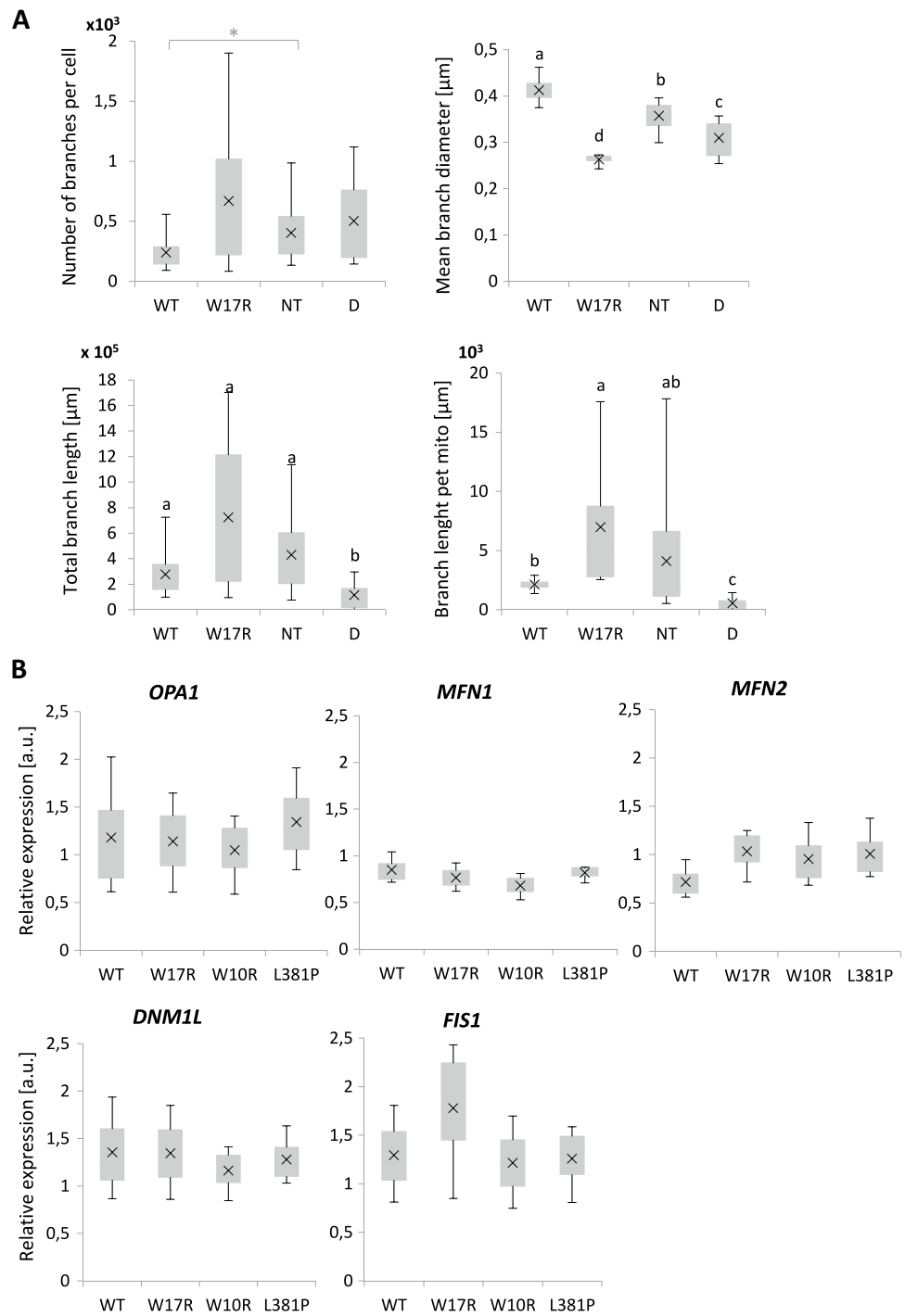
Fig. 6 Morphological analysis of mitochondria. **A** In the representative image, three distinct morphological categories of mitochondria are shown: rounded, tubular, and small. The graphs depict the percentage of cells with different morphological forms. In the graph different letters represent groups with statistically different values ($p < 0.05$), as determined by ANOVA with Games–Howell post hoc test. The results are presented as mean values ($n = 3 \pm SD$). **B** 3D morphological analysis was performed using ImageJ (Mitochondria Analyser) on the following cell lines: WT, W17R, NT (non-transduced HEK293T cells), and D (dividing cells from NT). The graphs display the mean number of mitochondria per cell, mean volume of mitochondria, mean surface area of mitochondria, and sphericity. Different letters represent groups with statistically different values ($p < 0.05$), as determined by ANOVA with Games–Howell post hoc test (group labeled as “ab” is different from neither “a” nor “b” groups). Data are presented as mean \pm SD values based on measurements from at least 5 individual cells in three independent experiments ($n = 3$)



line, a finding not previously reported for ADTKD-REN mutations. Recognized as noninvasive urinary ER stress biomarkers, MANF and CRELD2 proteins offer promising opportunities for early diagnosis and treatment monitoring in ADTKD-UMOD patients [33]. If the observed increases in their expression levels are validated in patients with renin mutations, they could also serve as diagnostic markers for ADTKD-REN. Our findings, confirming and expanding upon the molecular commonalities between ADTKD-UMOD and ADTKD-REN due to mutations in the mature part of renin, gain additional significance in the context of recent research by Kim et al., whose study highlights MANF's role in protecting kidney function in a mouse model of ADTKD-UMOD and suggests its potential as a biotherapeutic agent [34].

However, the implications for patients with signal sequence mutations are not as straightforward. The effect of these mutations on protein trafficking depends on how they impact the signal sequence, as demonstrated by early analyses of mutations such as L16R and L16del. While L16R prevented ER cotranslational translocation, L16del merely reduced it [10]. Our study indicates a similar pattern for W17R and W10R mutations. However, the relationship between these variations and ER stress activation remains unclear. ER stress can be triggered both by the accumulation of misfolded proteins within the ER and by aggregation events outside the ER [35, 36]. Although the L16del mutation showed signs of IRE1 pathway activation [10], it remains the only signal sequence mutation thoroughly investigated in this context. Our findings did not reveal ERS in the W17R cell line, and while the W10R mutation appeared

Fig. 7 Analysis of mitochondrial network. **A** 3D analysis of the mitochondrial network was conducted using ImageJ (Mitochondria Analyser) for the following cell lines: WT, W17R, NT (non-transduced HEK293T cells), and D (dividing cells from NT). The graphs illustrate the number of mitochondrial branches per cell, mean branch diameter, total branch length, and branch length per mitochondrion. Asterisk or different letters represent groups with statistically different values ($p < 0.05$), as determined by ANOVA with Games–Howell post hoc test. Data are presented as mean \pm SD based on three independent experiments ($n = 3$). **B** RT-qPCR analysis of fusion and fission markers. The graphs present the mean ($n = 3 \pm$ SD) relative mRNA expression of *OPA1* (OPA1 Mitochondrial Dynamin Like GTPase), *MFN1* (Mitofusin 1), *MFN2* (Mitofusin 2) as fusion markers, and *DNM1L* (Dynamin 1 Like) and *FIS1* (Fission, Mitochondrial1) as fission markers, all normalized to *HPRT1* (Hypoxanthine Phosphoribosyltransferase) and compared to WT cell line (Student's t-test). A.U. = arbitrary unit



to induce the PERK arm of the UPR, it was not accompanied by increased *BIP* expression, highlighting the need for further research.

The W17R renin mutation, altering the signal sequence and preventing effective ER translocation, results in its cytoplasmic localization. Considering that cytosolic renin (renin b), lacking an ER signal sequence, is partly directed towards mitochondria [2], we investigated W17R's subcellular localization and confirmed its partial mitochondrial misrouting.

These observations, independently corroborated by Schaeffer et al.'s studies showing more pronounced mitochondrial mistargeting [37], reinforce the hypothesis of possible mitochondrial involvement in ADTKD-REN pathogenesis. This finding, along with model-dependent variations in the severity of effects, emphasizes the need to examine patient samples for a comprehensive understanding.

Schaeffer et al. [37] highlighted mitochondrial network fragmentation as a potential cellular-level pathogenic

mechanism. In our experimental model, we observed similar disruptions in the mitochondrial network of the W17R line, specifically a decrease in tubular mitochondria and an increase in small mitochondria. However, our 3D analysis did not confirm classic network fragmentation; instead, it revealed a notable reduction in the average branch diameter of the ADTKD network compared to control groups. The absence of significant differences in the mRNA levels of genes involved in mitochondrial fission and fusion dynamics lends further credence to these findings. Such results underscore the necessity of employing 3D analysis in mitochondrial network studies and highlight the importance of conducting additional research to delineate the specific alterations caused by misdirected and damaged renin.

Further investigations into the role of mitochondria in ADTKD-REN pathogenesis may benefit from the established links between mitochondrial anomalies and TKD. Considering the hypothesis that mitochondrial tRNA^{Phe} malfunction leads to the ADTKD phenotype in MITKD [8], it is compelling to investigate how renin variants localized within mitochondria affect mitochondrial transcription and translation processes. This line of inquiry is reinforced by findings that the deletion of mitochondrial transcription factor A (TFAM) in mouse kidney tubule cells results in mitochondrial DNA leakage, triggering the STING (cyclic GMP–AMP synthase–stimulator of interferon genes) pathway and causing renal inflammation and fibrosis [38]. Additionally, recent theories suggest that disruptions in mitochondrial homeostasis, activating the STING pathway, may provide the missing link between ERS activation and fibrosis in ADTKD-UMOD pathogenesis [34]. This discovery is pivotal as it bridges a critical gap in our understanding of how ERS transitions to fibrosis, a previously unclear aspect of the disease mechanism. Moreover, since this process occurs at the mitochondrial level, it could represent a common pathway for both mutations that cause ERS and those that do not. Investigating whether this mechanism also plays a role in ADTKD-REN represents a significant direction for future research.

In conclusion, our research shows that while mutations causing ADTKD-REN may result in ERS activation, this is not a universal phenomenon. This suggests that if a common molecular mechanism underlies ADTKD-REN pathogenesis, it is more likely associated with mitochondrial dysfunction rather than ER stress. The potential of the MANF protein, given its crucial role in regulating mitophagy and mitochondrial homeostasis [34], as a therapeutic agent for diverse renin mutations, presents a promising avenue for future research. Currently, fludrocortisone remains the most effective treatment option for ADTKD-REN, as demonstrated by the stabilization of renal function in our patient with W17R mutation over a four-year treatment period without significant side effects. The scarcity of reports on

long-term fludrocortisone usage complicates the ability to conclude the treatment's universality among different mutation types and duration of renal protection across all ADTKD-REN cases. This gap underscores the importance of our report, contributing insights to the expanding body of knowledge on the subject.

Supplementary Information The online version contains supplementary material available at <https://doi.org/10.1007/s00467-024-06350-4>.

Acknowledgements The authors would like to thank Kinga Adamczyk-Węglarzy (Hirszfeld Institute of Immunology and Experimental Therapy, Polish Academy of Sciences; Laboratory of Molecular and Cellular Immunology, Wrocław, Poland), for her technical assistance.

Author contributions Conceptualization, A.Ł.; methodology, A.Ł., A.J., J.N.-T., M.M.; formal analysis and investigation, A.Ł., J.N.-T., A.J., M.M., M.P., M.C., A.M., K.K.-P., R.M.; writing—original draft preparation, A.Ł.; writing—review and editing, J.N.-T., A.J., M.M., M.P., A.M., K.K.-P., M.C., R.M.; funding acquisition, M.C., K.K.-P.; supervision, A.Ł..

Data availability The datasets generated and analysed during the current study are available from the corresponding author on reasonable request.

Declarations

Competing interests The authors have no relevant financial or non-financial interests to disclose.

Ethics approval All procedures performed in studies involving human participants were in accordance with the ethical standards of the institutional and/or national research committee and with the 1964 Helsinki Declaration and its later amendments or comparable ethical standards. The study was approved by the Bioethics Committee of the Medical University of Wrocław (No 413/2019).

References

- Mabillard H, Sayer JA, Olinger E (2023) Clinical and genetic spectra of autosomal dominant tubulointerstitial kidney disease. *Nephrol Dial Transplant* 38:271–282. <https://doi.org/10.1093/ndt/gfab268>
- Clausmeyer S, Stürzebecher R, Peters J (1999) An Alternative Transcript of the Rat Renin Gene Can Result in a Truncated Prorenin That Is Transported Into Adrenal Mitochondria. *Circ Res* 84:337–344. <https://doi.org/10.1161/01.RES.84.3.337>
- Clausmeyer S, Reinecke A, Farrenkopf R et al (2000) Tissue-Specific Expression of a Rat Renin Transcript Lacking the Coding Sequence for the Prefragment and Its Stimulation by Myocardial Infarction. *Endocrinology* 141:2963–2970. <https://doi.org/10.1210/endo.141.8.7623>
- Wanka H, Kefler N, Ellmer J et al (2009) Cytosolic renin is targeted to mitochondria and induces apoptosis in H9c2 rat cardiomyoblasts. *J Cell Mol Med* 13:2926–2937. <https://doi.org/10.1111/j.1582-4934.2008.00448.x>
- Wanka H, Lutze P, Staar D et al (2018) An alternative renin isoform is cardioprotective by modulating mitochondrial metabolism.

- J Cell Mol Med 22:5991–6001. <https://doi.org/10.1111/jcmm.13872>
6. Golchert J, Staar D, Bennewitz J et al (2022) Overexpression of Renin-B Induces Warburg-like Effects That Are Associated with Increased AKT/mTOR Signaling. *Cells* 11:1459. <https://doi.org/10.3390/cells11091459>
 7. Wanka H, Lutze P, Albers A et al (2021) Overexpression of transcripts coding for renin-b but not for renin-a reduce oxidative stress and increase cardiomyoblast survival under starvation conditions. *Cells* 10:1204. <https://doi.org/10.3390/cells10051204>
 8. Gubler MC, Antignac C (2010) Renin-angiotensin system in kidney development: Renal tubular dysgenesis. *Kidney Int* 77:400–406. <https://doi.org/10.1038/ki.2009.423>
 9. Živná M, Kidd K, Zaidan M et al (2020) An international cohort study of autosomal dominant tubulointerstitial kidney disease due to REN mutations identifies distinct clinical subtypes. *Kidney Int* 98:1589–1604. <https://doi.org/10.1016/j.kint.2020.06.041>
 10. Živná M, Hůlková H, Matignon M et al (2009) Dominant Renin Gene Mutations Associated with Early-Onset Hyperuricemia, Anemia, and Chronic Kidney Failure. *Am J Hum Genet* 85:204–213. <https://doi.org/10.1016/j.ajhg.2009.07.010>
 11. Ke B, Zhu N, Luo F et al (2017) Targeted inhibition of endoplasmic reticulum stress: New hope for renal fibrosis (Review). *Mol Med Rep* 16:1014–1020. <https://doi.org/10.3892/mmr.2017.6762>
 12. Marciniak SJ, Chambers JE, Busija D (2022) Pharmacological targeting of endoplasmic reticulum stress in disease. *Nat Rev Drug Discov* 21:115–140. <https://doi.org/10.1038/s41573-021-00320-3>
 13. Schaeffer C, Izzi C, Vettori A et al (2019) Autosomal Dominant Tubulointerstitial Kidney Disease with Adult Onset due to a Novel Renin Mutation Mapping in the Mature Protein. *Sci Rep* 9:11601. <https://doi.org/10.1038/s41598-019-48014-6>
 14. Connor TM, Hoer S, Mallett A et al (2017) Mutations in mitochondrial DNA causing tubulointerstitial kidney disease. *PLoS Genet* 13:e1006620. <https://doi.org/10.1371/journal.pgen.1006620>
 15. Bleyer AJJ, Živná M, Hůlková H et al (2010) Clinical and molecular characterization of a family with a dominant renin gene mutation and response to treatment with fludrocortisone. *Clin Nephrol* 74:411–422. <https://doi.org/10.5414/cnp74411>
 16. Teufel F, Armenteros JJA, Johansen AR et al (2022) SignalP 6.0 predicts all five types of signal peptides using protein language models. *Nat Biotechnol* 40:1023–1025. <https://doi.org/10.1038/s41587-021-01156-3>
 17. Walczak-Drzewiecka A, Ratajewski M, Wagner W, Dastych J (2008) HIF-1 α Is Up-Regulated in Activated Mast Cells by a Process That Involves Calcineurin and NFAT. *J Immunol* 181:1665–1672. <https://doi.org/10.4049/jimmunol.181.3.1665>
 18. Silver RB, Reid AC, Mackins CJ et al (2004) Mast cells: A unique source of renin. *Proc Natl Acad Sci U S A* 101:13607–13612. <https://doi.org/10.1073/pnas.0403208101>
 19. Suchanski J, Tejchman A, Zacharski M et al (2017) Podoplanin increases the migration of human fibroblasts and affects the endothelial cell network formation: A possible role for cancer-associated fibroblasts in breast cancer progression. *PLoS One* 12:e0184970. <https://doi.org/10.1371/journal.pone.0184970>
 20. Dull T, Zufferey R, Kelly M et al (1998) A Third-Generation Lentivirus Vector with a Conditional Packaging System. *J Virol* 72:8463–8471. <https://doi.org/10.1128/JVI.72.11.8463-8471.1998>
 21. Wang Y, Shen J, Arenzana N et al (2000) Activation of ATF6 and an ATF6 DNA binding site by the ER stress response Yan. *J Biol Chem* 275:27013–27020. [https://doi.org/10.1016/S0021-9258\(19\)61473-0](https://doi.org/10.1016/S0021-9258(19)61473-0)
 22. Harding HP, Novoa I, Zhang Y et al (2000) Regulated Translation Initiation Controls Stress-Induced Gene Expression in Mammalian Cells. *Mol Cell* 6:1099–1108. [https://doi.org/10.1016/s1097-2765\(00\)00108-8](https://doi.org/10.1016/s1097-2765(00)00108-8)
 23. Jheng JR, Lau KS, Tang WF et al (2010) Endoplasmic reticulum stress is induced and modulated by enterovirus 71. *Cell Microbiol* 12:796–813. <https://doi.org/10.1111/j.1462-5822.2010.01434.x>
 24. Bolte S, Cordelières FP (2006) A guided tour into subcellular colocalization analysis in light microscopy. *J Microsc* 224:213–232. <https://doi.org/10.1111/j.1365-2818.2006.01706.x>
 25. Schindelin J, Arganda-Carrera I, Frise E et al (2012) Fiji - an Open platform for biological image analysis. *Nat Methods* 28:676–682. <https://doi.org/10.1038/nmeth.2019>
 26. Chaudhry A, Shi R, Luciani DS (2020) A pipeline for multidimensional confocal analysis of mitochondrial morphology, function and dynamics in pancreatic β -cells. *Am J Physiol Endocrinol Metab* 318:87–101. <https://doi.org/10.1152/ajpendo.00457.2019>
 27. Chaudhry A. Mitochondria Analyzer (Online). <https://github.com/AhsenChaudhry/Mitochondria-Analyzer>. Accessed Apr 2023
 28. Osowski CM, Urano F (2011) Measuring ER stress and the unfolded protein response using mammalian tissue culture system. *Methods Enzymol* 490:71–92. <https://doi.org/10.1016/B978-0-12-385114-7.00004-0>
 29. Taguchi N, Ishihara N, Jofuku A et al (2007) Mitotic phosphorylation of dynamin-related GTPase Drp1 participates in mitochondrial fission. *J Biol Chem* 282:11521–11529. <https://doi.org/10.1074/jbc.M607279200>
 30. Suh J, Kim NK, Shim W et al (2023) Mitochondrial fragmentation and donut formation enhance mitochondrial secretion to promote osteogenesis. *Cell Metab* 35:345–360.e7. <https://doi.org/10.1016/j.cmet.2023.01.003>
 31. Dabrowska A, Venero JL, Iwasawa R et al (2015) PGC-1 α controls mitochondrial biogenesis and dynamics in lead- induced neurotoxicity. *Aging (Albany NY)* 7:629–643. <https://doi.org/10.18632/aging.100790>
 32. Dvela-Levitt M, Shaw JL, Greka A (2021) A Rare Kidney Disease To Cure Them All? Towards Mechanism-Based Therapies for Proteinopathies. *Trends Mol Med* 27:394–409. <https://doi.org/10.1016/j.molmed.2020.11.008>
 33. Park SJ, Kim Y, Chen YM (2019) Endoplasmic reticulum stress and monogenic kidney diseases in precision nephrology. *Pediatr Nephrol* 34:1493–1500. <https://doi.org/10.1007/s00467-018-4031-2>
 34. Kim Y, Li C, Gu C et al (2023) MANF stimulates autophagy and restores mitochondrial homeostasis to treat autosomal dominant tubulointerstitial kidney disease in mice. *Nat Commun* 14:6493. <https://doi.org/10.1038/s41467-023-42154-0>
 35. Ogen-Shtern N, Ben David T, Lederkremer GZ (2016) Protein aggregation and ER stress. *Brain Res* 1648:658–666. <https://doi.org/10.1016/j.brainres.2016.03.044>
 36. Vidak S, Serebryanny LA, Pegoraro G, Misteli T (2023) Activation of endoplasmic reticulum stress via clustering of the inner nuclear membrane protein SUN2. *Cell Rep* 42:112534. <https://doi.org/10.1101/2021.09.14.460295>
 37. Schaeffer C, De Fusco M, Pasqualetto E et al (2023) Leader peptide or pro-segment mutants of renin are misrouted to mitochondria in autosomal dominant tubulointerstitial kidney disease. *Dis Model Mech* 16:dmm049963. <https://doi.org/10.1242/dmm.049963>
 38. Wung Chung K, Dhillon P, Huang S et al (2019) Mitochondrial Damage and Activation of the STING Pathway Lead to Renal Inflammation and Fibrosis. *Cell Metab* 30:784–799. <https://doi.org/10.1016/j.cmet.2019.08.003>

Publisher's Note Springer Nature remains neutral with regard to jurisdictional claims in published maps and institutional affiliations.

Springer Nature or its licensor (e.g. a society or other partner) holds exclusive rights to this article under a publishing agreement with the author(s) or other rightsholder(s); author self-archiving of the accepted manuscript version of this article is solely governed by the terms of such publishing agreement and applicable law.